

2627

NRL Report 7420

UNCLASSIFIED

Statistical Functions of Short-Pulse Radar Sea Return

K. R. SCHMIDT, P. M. THIEBAUD, AND S. J. WELLER

*Search Radar Branch
Radar Division*

July 26, 1972



NAVAL RESEARCH LABORATORY
Washington, D.C.

Approved for public release: distribution unlimited.

DDe-A

CONTENTS

Abstract	ii
Authorization	ii
INTRODUCTION	1
AIRBORNE SEA-RETURN DISTRIBUTIONS AT 5-DEGREE GRAZING ANGLES	2
VERY-LOW-ANGLE SHORE-BASED SEA- RETURN DISTRIBUTIONS	9
NANOSECOND RADAR OBSERVATIONS OF SWIMMING-POOL CLUTTER	9
AUTOCORRELATION OF SEA RETURN	10
CONCLUSIONS AND FINAL REMARKS	15
ACKNOWLEDGMENTS	16
REFERENCES	16

ABSTRACT

This report presents and discusses experimental results of short-pulse (20 and 100 nsec) X-band radar backscatter measurements from rough water surfaces. The emphasis is on airborne open-ocean conditions, but some results from very-low-angle shore-based data and 1-nanosecond radar measurements in the NRL swimming pool are also shown. The experimental data are in the form of cumulative probability distribution functions and autocorrelation functions. Among the various conclusions drawn are that the non-Rayleigh character of the data cannot be adequately explained by a composite surface which consists of a slightly rough, ideal Gaussian random surface superimposed upon a wave structure whose crest-to-trough amplitude is very large compared to a radar wavelength. The pool clutter results indicate that such a large wave structure is not necessary to obtain data which are considerably more skewed than Rayleigh. Additional wave-tank measurements should be made to gain insight as to the effects of the variation of many of the parameters which in the present study remained fixed.

AUTHORIZATION

NRL Problem R02-34A
Project RF 12-151-403-4008

Manuscript submitted March 31, 1972.

STATISTICAL FUNCTIONS OF SHORT-PULSE RADAR SEA RETURN

INTRODUCTION

Most often in determining various electrical or geometrical properties of some particular rough surface, the surface is not conveniently accessible, and some type of electromagnetic propagation technique is employed. Usually in electromagnetic probing, or remote sensing as it is sometimes called, it is the backscattered return that is recorded, due to experimental convenience rather than to any rigid theoretical reasons. By analyzing the return, conclusions are drawn as to the nature of the surface.

As is pointed out in Chapter 3 of Ref. 1, this situation is the inverse of the boundary-value problem in classical electromagnetic theory. With the latter a surface (boundary between two media) is specified and the resulting field distribution is calculated (at least in theory) by satisfying the boundary conditions. The result is unique; for a given set of boundary conditions, a unique field distribution is calculated. With the probing situation, however, there is no known way of obtaining a unique surface which produced a given set of data. Yet in many practical applications it is possible, by a rather thorough analysis of the data, to ascertain many of the properties of the remote surface.

In pulse radar work, since the surface almost always completely fills the beam, the average returned power is expressed in terms of an average echo area (cross section) per patch area, and is designated σ_0 . To measure σ_0 , a rather accurately known calibrated reference target must be used. In practice it is often difficult if not impossible to place a level of accuracy on the measured values of σ_0 . Even if σ_0 were known exactly, other major limitations would remain. In radar detection, for example, one must know the probability density function of the "clutter" in order to estimate a false alarm rate for a given operating threshold level. That is, what is required is the complete *shape* of the dispersion about the mean amplitude value rather than just the mean square of the amplitude, which is proportional to σ_0 . As a second example, in the particular remote sensing application of determining the complex dielectric properties of a rough surface, it has been found that polarization-dependent studies yield more meaningful results than those obtained by simply measuring average backscattered power at several frequencies. More details may be found in Refs. 1 and 2.

The present report is concerned with short-pulse (high-resolution) radar reflections from the ocean surface. In particular, the postdetected (noncoherent) amplitude is examined sample by sample and the cumulative probability distributions and autocorrelation functions of the amplitude values are presented. The raw data are essentially those used in Ref. 3, but in the latter we were almost exclusively concerned about possible long-term time-varying trends in the data (usually either periodic components or transient phenomenon). A few distributions were obtained however, and it appeared that somewhat of a pattern was developing with regard to their shapes as polarization, wind direction, pulse width, etc. were changed. Consequently it was felt that a more thorough

investigation should be made with regard to distributions and autocorrelation functions. To understand the need for these two categories of experimental data, it is necessary to have some familiarity with the history of ocean surface backscatter.

Although "sea return" has been measured for many years, only relatively recently have functions such as distributions and correlations of sea return been tabulated and analyzed. Prior to this it was customary to measure σ_0 , which resulted in a number instead of a function. There are probably several reasons for this. First of all, earlier radars operated with pulse lengths in the range of microseconds or tens of microseconds and thus illuminated a large area. Experimentalists observing A-scope traces of clutter saw a waveform which was usually not unlike that for thermal noise. It was rightly concluded that the postdetected clutter envelope possessed a Rayleigh distribution. Knowing this, it was logical that σ_0 was what was measured as a function of grazing angle, polarization, frequency, etc. Even if the distribution were not Rayleigh, one could not have done much, because data storage and display capabilities were not conducive to handling millions of data samples.

When shorter pulses (high resolution) became a reality, however, the A-scope traces no longer had the random-noiselike appearance as before but exhibited what has now become known as spiky characteristics. While similar in appearance to random noise, these waveforms possessed relatively infrequent but large amplitude spikes. The probability distribution of these amplitudes was clearly non-Rayleigh, the probability of observing much larger amplitudes being much higher than for a Rayleigh population. Even though digital tape capabilities were still not such that experimental histograms could be generated, it became clear that clutter in many cases could no longer be explained as consisting simply of a "large number of independent scatterers."

Despite this radical departure from Gaussian statistics and the obviously implied increased difficulties with the detection of small targets, the statistical functions (distributions and autocorrelation) of sea return have not always had a very thorough treatment. This is one of the principal motivations for the research summarized in this report. In addition to target detection, the area of remote sensing constitutes a second application of the possible use of these functions. In the case of sea return it is not obvious how the distribution varies with sea state, even though it is fairly well established that σ_0 experiences a saturation effect for increasing ocean roughness (4). However, with the results to be presented here we will be able to draw some conclusions with regard to differences in the distributions for different wind directions.

The bulk of this report is concerned with the composite representative results of the cumulative distributions and autocorrelation functions of about 85 2-minute runs of short-pulse (20 and 100 nsec) sea return taken from an airborne platform. A few comparisons are made with some experimental data taken with a nanosecond radar in conjunction with waves generated by a fan and paddle in the NRL swimming pool. Some data taken from the shore at Boca Raton, Florida, involving a very low grazing angle (about 0.3°) is also discussed.

AIRBORNE SEA-RETURN DISTRIBUTIONS AT 5-DEGREE GRAZING ANGLES

Several years ago NRL developed a new frequency-agile short-pulse (20 nsec) X-band radar to be used primarily for recording the pulse-by-pulse sea return from an airborne

platform. (Reference 5 gives hardware details of the radar.) In addition to the newly incorporated frequency-agility feature the radar had a considerably wider dynamic range than was obtained previously. Hence the distribution curves to be presented have appreciably greater accuracy in the region of higher power level than they would have had in that region for previous radars, which is the area of greatest interest as far as false alarms are concerned.

During the spring of 1969 the radar was flown over the Atlantic approximately 100 miles east of the Maryland shore. Some of the various properties of the sea-return results have been documented previously. For example, in Ref. 6 the effects of frequency diversity on the correlation functions were discussed. In Ref. 3 the results of time-trend analyses were presented. It was concluded that over time intervals of from 30 seconds to 2 minutes there existed no appreciable long-term transient phenomena or periodic components. It was necessary to determine this before presenting a large number of the distribution functions, because a 2-minute histogram is rather meaningless if the random process which generated it contains these time-varying properties.

For the 1969 data the radar parameters and the various conditions under which the flights were conducted are shown in Table 1. More information on the flight procedures together with details on the digitizing of the data can be found in Ref 3. From Table 1 the variable quantities are pulse width, direction of flight, polarization, and sea state. The terms used to indicate sea state are extremely qualitative, because, although the information was obtained from the Fleet Weather Facility, we are not sure whether a fully developed sea was present.

The resulting distributions are shown in Figs. 1, all of which are plotted to the same relative decibel scale. Since calibration runs were made frequently, information with regard to absolute power levels was preserved; this accounts for the varying positions of the

Table 1
Experimental Details and Radar Parameters
for the Data Obtained from an Airborne Platform

Frequency:	9250 MHz (nominal)			
Pulse widths:	20 nsec and 100 nsec			
Pulse repetition frequency:	1.28 kHz			
Antenna beamwidth:	7° vertical and 0.5° horizontal			
Polarization:	linear, vertical, or horizontal			
Aircraft altitude:	1000 feet			
Aircraft velocity:	180 knots			
Slant range:	2 nautical miles			
Grazing angle (angle with horizontal):	5°			
Radar Patch Sizes:	10 by 120 feet (20-nsec pulse) 50 by 120 feet (100-nsec pulse)			
Antenna:	fixed in a forward-looking direction			
Dates of measurements:	March 5, 11, and 12, 1969			
Location:	71°W, 38°N, or about 275 miles due east of the Patuxent River Naval Station, Maryland			
Approximate Sea Conditions:				
	March Date	Wind (knots)	Wind Waves (crest to trough)	Swell (feet)
	5	9-14	4	8
	11	26-31	7	12
	12	38-43	8	33
Directions of measurements:	upwind, downwind, and crosswind*			

*There were no crosswind flights on March 5.

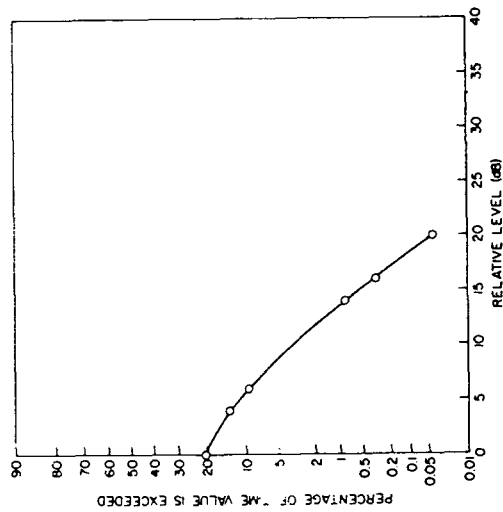


Fig. 1a—Amplitude distribution of downwind moderate-sea return of horizontally polarized 20-nanosecond pulses at a 5° grazing angle

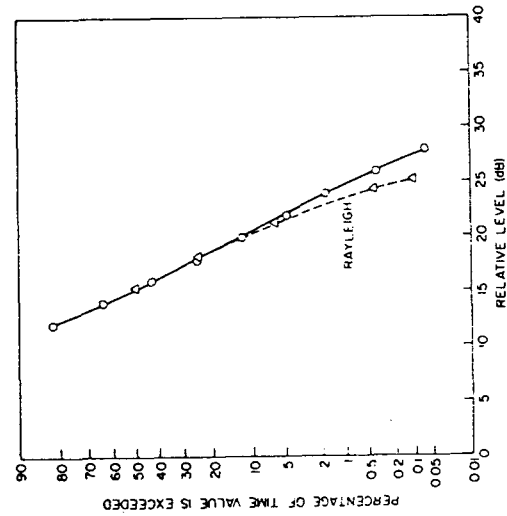


Fig. 1d—Amplitude distribution of upwind moderate-sea return of vertically polarized 20-nanosecond pulses at a 5° grazing angle

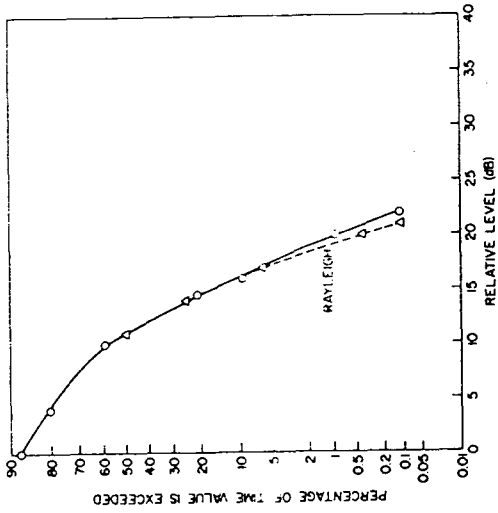


Fig. 1b—Amplitude distribution of downwind moderate-sea return of vertically polarized 20-nanosecond pulses at a 5° grazing angle

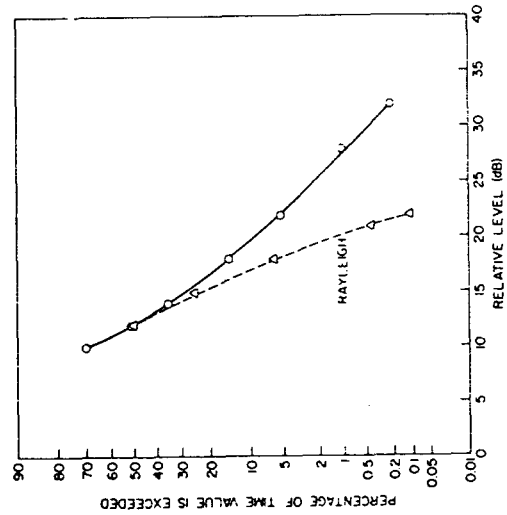


Fig. 1e—Amplitude distribution of downwind moderate-sea return of horizontally polarized 100-nanosecond pulses at a 5° grazing angle

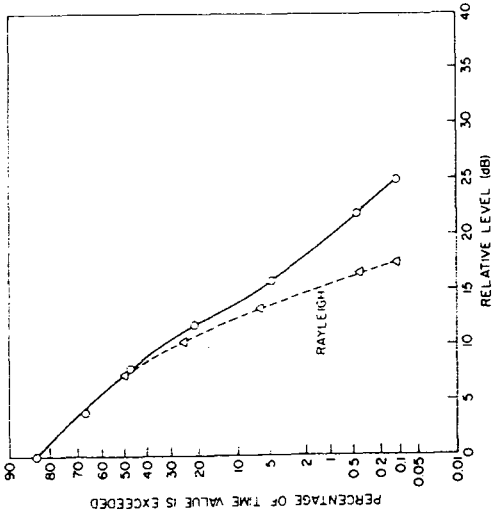


Fig. 1c—Amplitude distribution of upwind moderate-sea return of horizontally polarized 20-nanosecond pulses at a 5° grazing angle

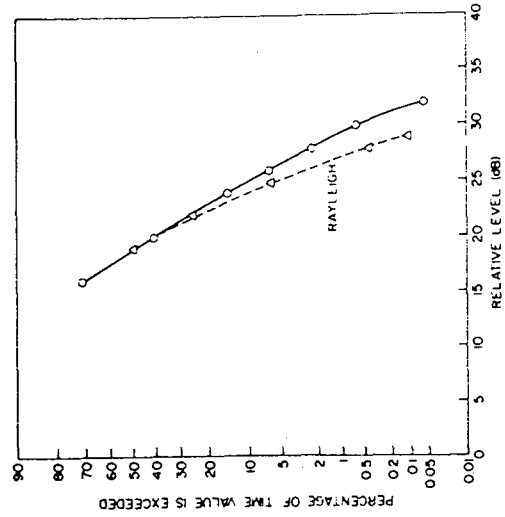


Fig. 1f—Amplitude distribution of downwind moderate-sea return of vertically polarized 100-nanosecond pulses at a 5° grazing angle

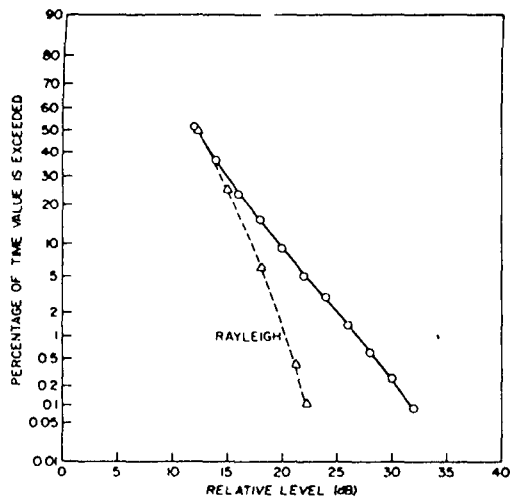


Fig. 1g—Amplitude distribution of upwind moderate-sea return of horizontally polarized 100-nanosecond pulses at a 5° grazing angle

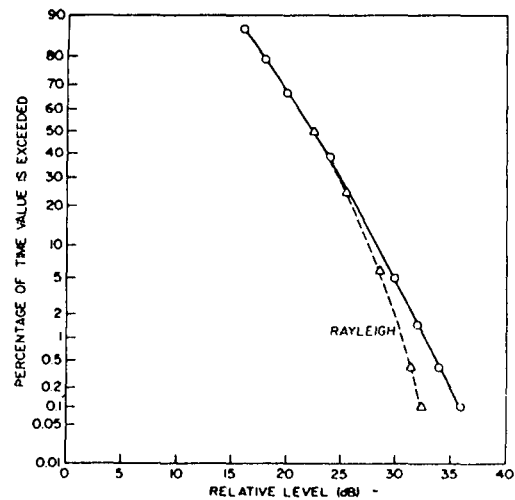


Fig. 1h—Amplitude distribution of upwind moderate-sea return of vertically polarized 100-nanosecond pulses at a 5° grazing angle

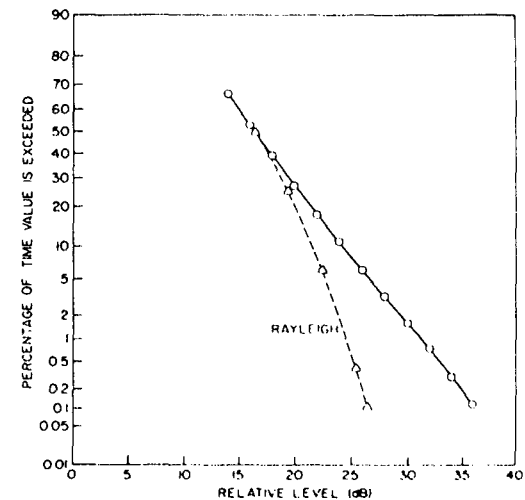


Fig. 1i—Amplitude distribution of downwind rough-sea return of horizontally polarized 100-nanosecond pulses at a 5° grazing angle

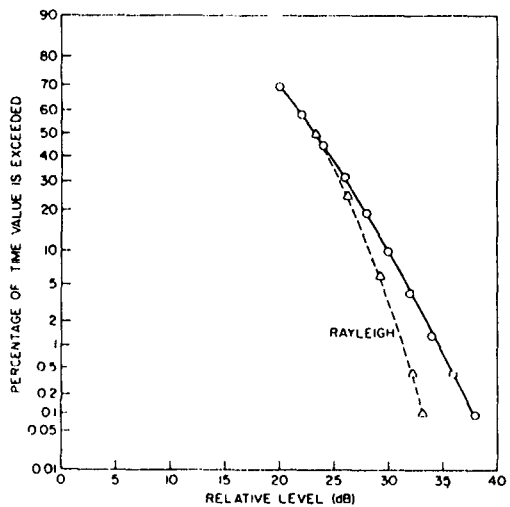


Fig. 1j—Amplitude distribution of downwind rough-sea return of vertically polarized 100-nanosecond pulses at a 5° grazing angle

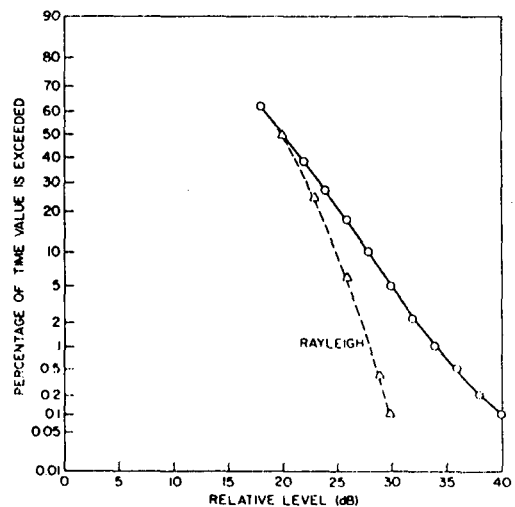


Fig. 1k—Amplitude distribution of upwind rough-sea return of horizontally polarized 100-nanosecond pulses at a 5° grazing angle

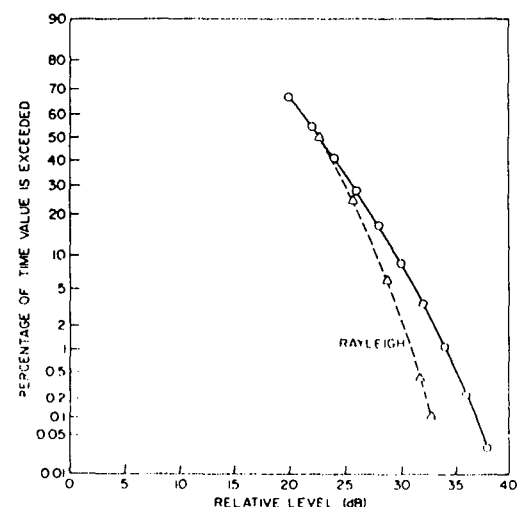


Fig. 1l—Amplitude distribution of upwind rough-sea return of vertically polarized 100-nanosecond pulses at a 5° grazing angle

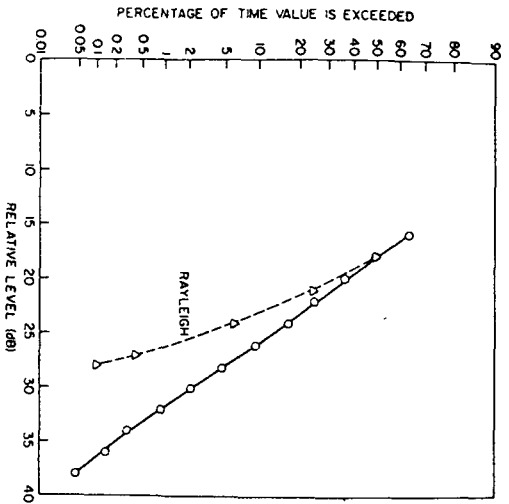


Fig. 1m—Amplitude distribution of crosswind rough-sea return of horizontally polarized 100-nanosecond pulses at a 5° grazing angle

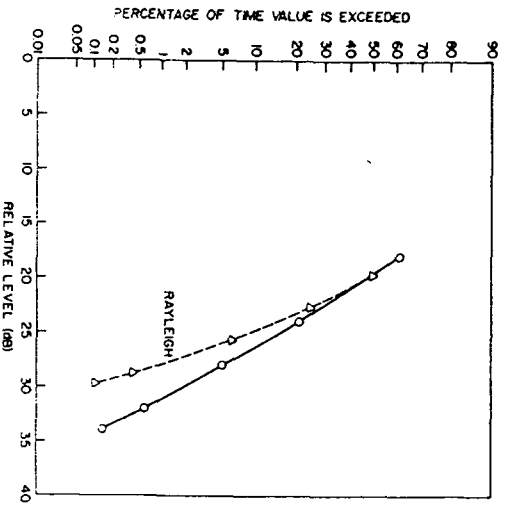


Fig. 1n—Amplitude distribution of crosswind rough-sea return of vertically polarized 100-nanosecond pulses at a 5° grazing angle

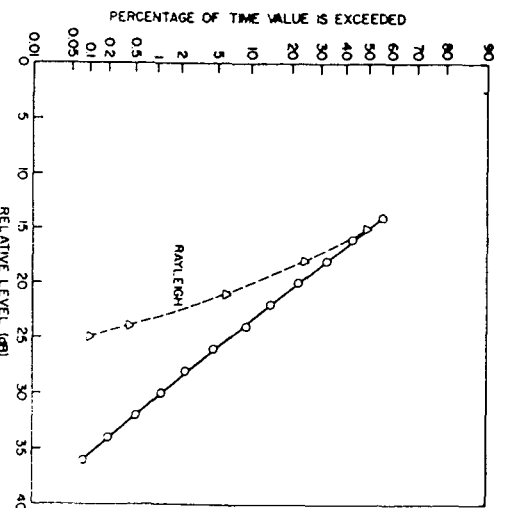


Fig. 1o—Amplitude distribution of crosswind very-rough-sea return of horizontally polarized 100-nanosecond pulses at a 5° grazing angle

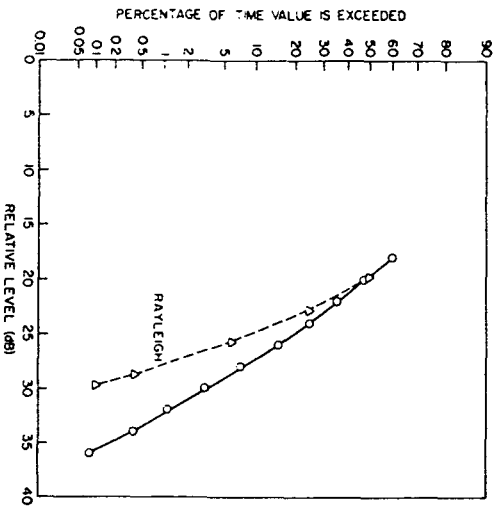


Fig. 1p—Amplitude distribution of crosswind very-rough-sea return of vertically polarized 100-nanosecond pulses at a 5° grazing angle

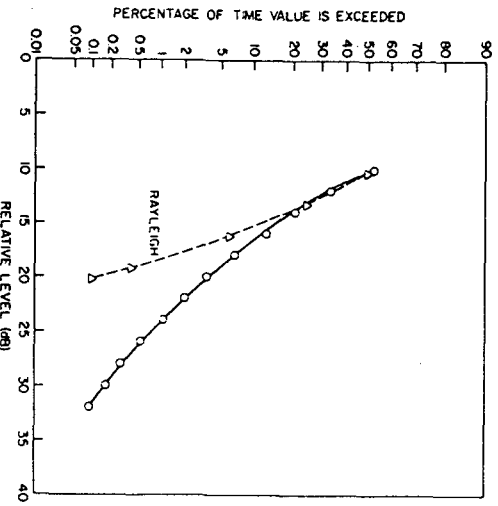


Fig. 1q—Amplitude distribution of downwind very-rough-sea return of horizontally polarized 20-nanosecond pulses at a 5° grazing angle

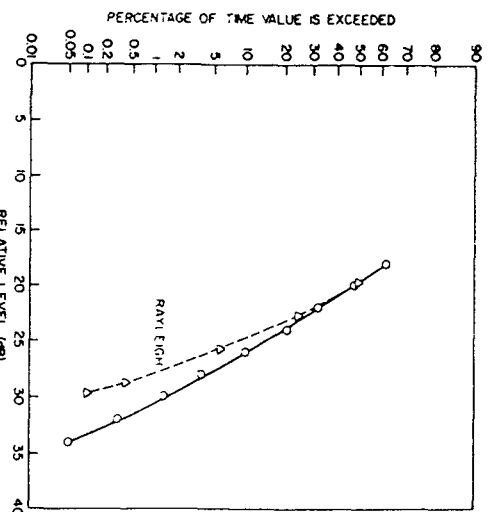


Fig. 1r—Amplitude distribution of downwind very-rough-sea return of vertically polarized 20-nanosecond pulses at a 5° grazing angle

Fig. 1s—Amplitude distribution of upwind very-rough-sea return of horizontally polarized 20-nanosecond pulses at a 5° grazing angle

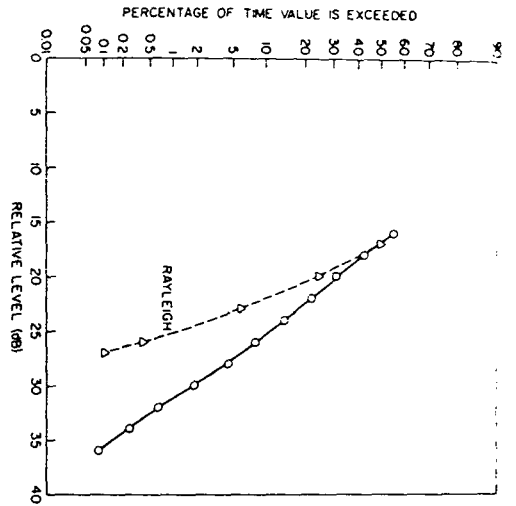


Fig. 1t—Amplitude distribution of vertically polarized very-rough-sea return of horizontally polarized 20-nanosecond pulses at a 5° grazing angle

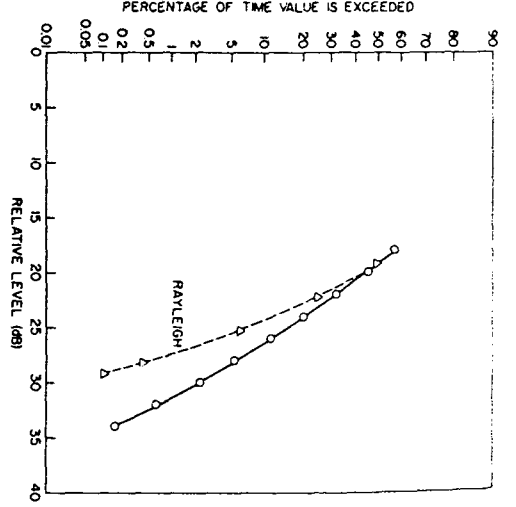


Fig. 1u—Amplitude distribution of crosswind very-rough-sea return of horizontally polarized 20-nanosecond pulses at a 5° grazing angle

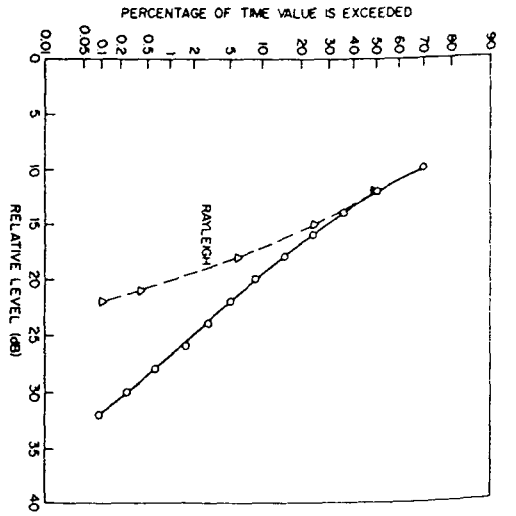


Fig. 1v—Amplitude distribution of crosswind very-rough-sea return of vertically polarized 20-nanosecond pulses at a 5° grazing angle

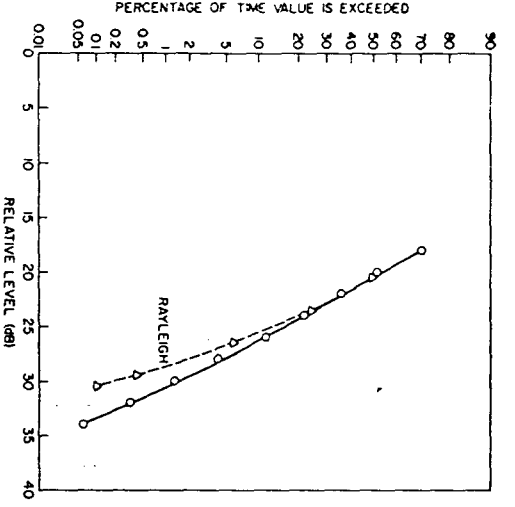
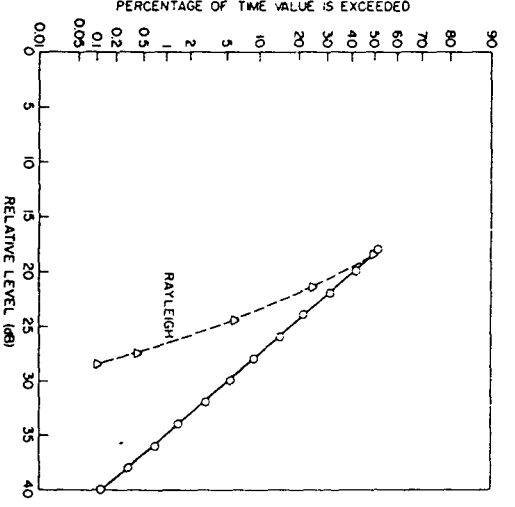


Fig. 1w—Amplitude distribution of upwind very-rough-sea return of horizontally polarized 100-nanosecond pulses at a 5° grazing angle



curves along the horizontal axis. For example, in Fig. 1d the 50% probability level of the data is about 8 dB higher than in Fig. 1c. It will also be noticed that most of the longer pulse cases (100 nsec) lie about 7 dB to the right of the corresponding 20-nsec ones, reflecting the 5-to-1 difference in patch size. Additionally, some measure of the skewness of the data can be obtained by a comparison of the curves with the Rayleigh amplitude distribution. In all cases the dynamic range in decibels to the right of the 50% point is always larger for the data than for the Rayleigh curve. This is even more so for horizontal polarization than for vertical polarization. For downwind and upwind conditions, the data curves are quite similar. For crosswind conditions, however, especially vertical polarization, the departure from the Rayleigh condition is not nearly as great.

As there exists a dynamic range of nearly 10 dB for the Rayleigh distribution between the 50% and the 0.1% probability levels, the decibel spread for the sea-return curves between these same points can be tabulated conveniently as a quantitative measure of the departure from the Rayleigh case. These are shown in Table 2.

The receiver average noise power level was about 0 dB on the horizontal axis; hence the ratio of sea return to noise is sufficiently high so that most of the distribution curves largely reflect sea return only and not sea return plus noise. The only exception is Fig. 1a, and we would be inclined to question its accuracy.

Table 2
Dynamic Range of the Data of Figs. 1 Between the 50% and the 0.1%
Probability Levels (Dynamic Range of the Rayleigh Distribution
is Nearly 10 dB)

Direction	Range (dB) and Figure Numbers in Parentheses					
	Moderate Sea*		Rough Sea†		Very Rough Sea‡	
	20-nsec Pulses	100-nsec Pulses	20-nsec Pulses	100-nsec Pulses	20-nsec Pulses	100-nsec Pulses
Horizontal Polarization						
Downwind	— (1a)	22.0 (1e)	—	19.5 (1i)	21.0 (1q)	—
Upwind	17.5 (1c)	19.0 (1g)	—	20.0 (1k)	18.5 (1s)	21.5 (1w)
Crosswind	—	—	—	18.5 (1m)	20.0 (1u)	20.5 (1o)
Vertical Polarization						
Downwind	11.0 (1b)	12.5 (1f)	—	15.0 (1j)	16.0 (1r)	—
Upwind	12.0 (1d)	13.5 (1h)	—	14.0 (1l)	15.0 (1t)	—
Crosswind	—	—	—	14.5 (1n)	13.0 (1v)	13.5 (1p)

*Sea conditions of March 5 in Table 1.

†Sea conditions of March 11 in Table 1.

‡Sea conditions of March 12 in Table 1.

VERY-LOW-ANGLE SHORE-BASED SEA-RETURN DISTRIBUTIONS

Although most of the curves in Figs. 1 indicate a rather radical departure from the Rayleigh distribution, there is experimental evidence that none of them represents the most extreme possibility. At grazing angles much lower than 5° (such as angles of 1° or less) the distribution of the sea return is much more skewed.

Figure 2, which is taken from Ref. 7, is one example of sea return taken from the Georgia Tech tower on the shore at Boca Raton, Florida, with a 0.3° grazing angle. Although this example may still not represent the worst case, it shows that in many practical applications of detecting small targets near the radar horizon the false-alarm problem can be severe. However, the average value (or σ_0) is not known for Fig. 2; thus it is impossible to give an exact comparison between the very-low-angle case and the airborne 5° curves in Figs. 1. The enormous degree of skewness can be appreciated by comparing the 31dB dynamic range between the 50% and the 0.1% probability levels with the airborne values in Table 2. The former exceeds any of the latter in all cases by at least 9 dB.

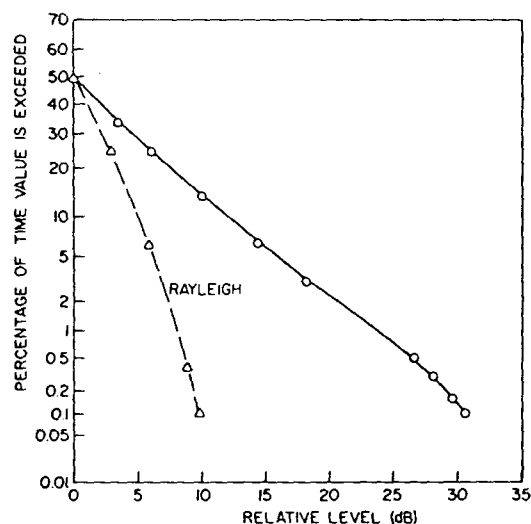


Fig. 2—Amplitude distribution of a 12-knot-wind-sea return of vertically polarized 100-nanosecond pulses at a very low grazing angle (0.3°)

NANOSECOND RADAR OBSERVATIONS OF SWIMMING-POOL CLUTTER

For several years NRL has had a research effort concerned with observing radar return from various types of wave structures in the NRL swimming pool. Fan-generated waves with wavelengths of about 3 centimeters or less have been considered and also a combination of these waves with those generated by a paddle, which are about 45 centimeters or so. Thus at X band the wavelength of the fan-only waves is of the order of a radar wavelength or smaller. With a 1-nanosecond pulse the resolution is less than the wavelength of

the paddle-generated waves. Under these conditions, it has been reported (7) that σ_0 values are close to those for open ocean for grazing angles between 5 and 80 degrees. This being the case, it was felt desirable to investigate the cumulative probability distributions for this type of pool clutter. With the fan-only waves having a structure (Fig. 3) which consists of several wave crests within the resolution cell, one might expect the resulting distribution of the radar return to be Rayleigh.

The results are shown in Fig. 4 and indicate that the distribution is not Rayleigh. This result is important because present-day sea-return modeling efforts are based on the assumption that the ocean surface looks like a fine capillary wave structure superimposed upon a much larger wave pattern. An additional assumption is also made that the fine structure of the surface height has a Gaussian distribution. The results in Fig. 4 and the corresponding time series shown in Fig. 5 indicate that for nanosecond pulses, it is not necessary to have a large (compared to the radar wavelength) wave structure in order to obtain data which is more skewed than Rayleigh, and that capillary wave heights whose amplitude is of the order of a radar wavelength or smaller do not obey the conditions for a random, Gaussian surface. Indeed it is well documented (8) that a water surface height is only approximately Gaussian, and in the case of short-pulse radar the size of the illuminated area may be small enough such that there is a high degree of correlation among many of the scatterers within the range cell. Figure 6 shows a time series of some output Rayleigh-distributed receiver noise, and it is clear that the time series in Fig. 5a has a much more skewed distribution than the former. The dynamic ranges between the 50% and the 0.1% probability levels in Fig. 4 are 12.5 dB for the fan only and 15.5 dB for the fan plus paddle as compared with a 10-dB dynamic range for the Rayleigh distribution. Thus, even for the fine capillary wave structure in the absence of any paddle waves, the return is not Rayleigh.

What is needed to properly explain the properties of sea return is a model considerably more advanced than the rather elementary concept of a large wave structure simply tilting a highly idealized random Gaussian surface.

AUTOCORRELATION OF SEA RETURN

The spatial correlation of sea return is defined as the crosscorrelation between the signals returned simultaneously from two separate patches of the sea in the radial dimension (9). Although the airborne experiments described in this report were not such that this crosscorrelation could be computed directly, it seems reasonable to assume that for several hundred milliseconds the ocean surface can be considered frozen. Under this assumption the time samples of the data described in this report can be used to calculate a reliable estimate of the spatial correlation of the return, at least for lags up to about 50 milliseconds. In Figs. 7 are shown the normalized correlation curves computed for lags up to 110 milliseconds from record lengths of 500 milliseconds. The corresponding distribution functions are shown in Figs. 8.

For a pulse width of 20 nanoseconds and an airplane speed of 180 knots, about 33 milliseconds are required to travel a range displacement equal to one pulse width. Previous results of others (9) indicate that the return is decorrelated at a range displacement equal to one pulse width for frequencies at S band and lower and pulse widths larger than 100 nanoseconds. However, for the same pulse widths and C-band frequencies, it has been shown (9) that the correlation function possesses a long tail for range displacements in excess of one pulse width. It was this characteristic at the higher frequencies plus the

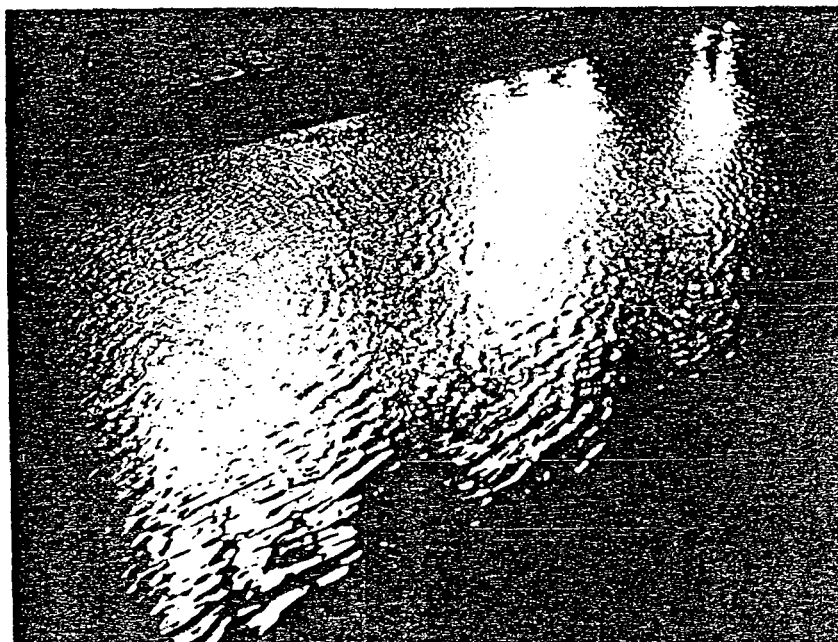


Fig. 3—Fan-generated waves of about 3 centimeters or less in the NRL swimming pool

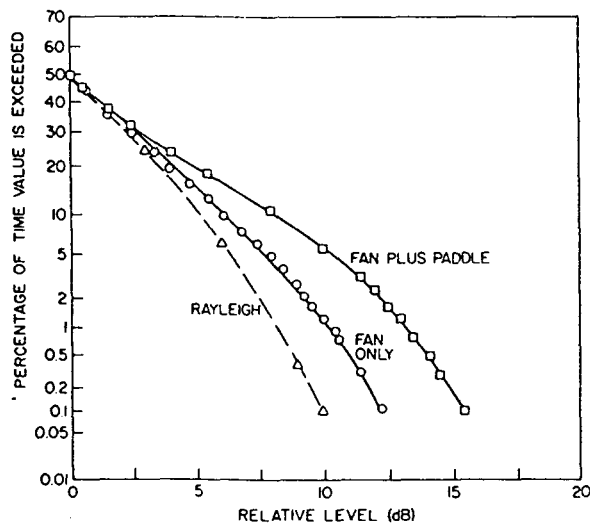
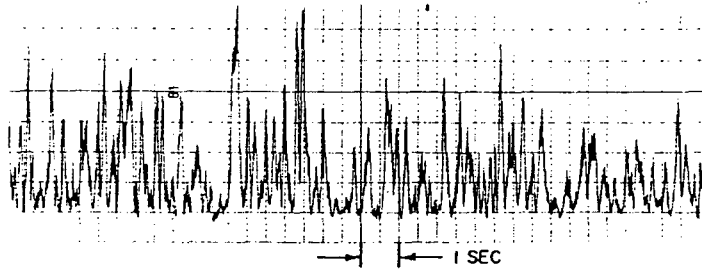
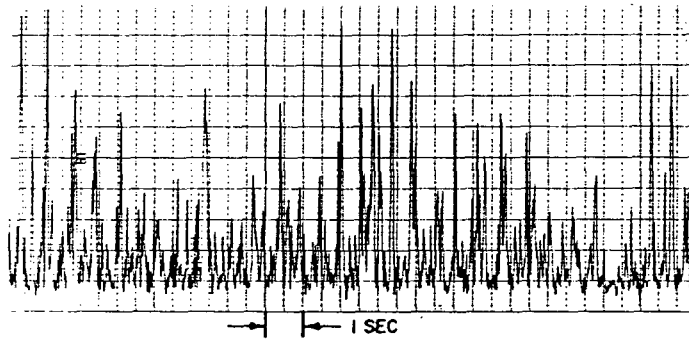


Fig. 4—Amplitude distributions of swimming-pool return of vertically polarized 1.2-nanosecond pulses at a 20° grazing angle. These distributions of swimming-pool clutter are typical of ten runs.



(a) Fan-generated waves only



(b) Fan-generated plus paddle-generated waves

Fig. 5—Postdetected swimming pool clutter

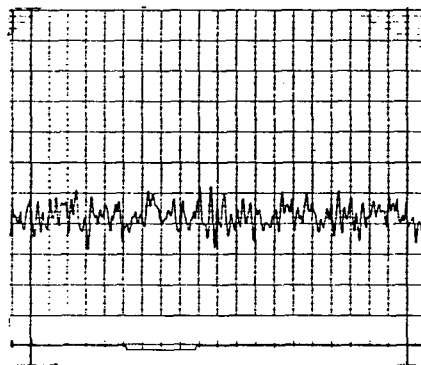


Fig. 6—Rayleigh-distributed noise

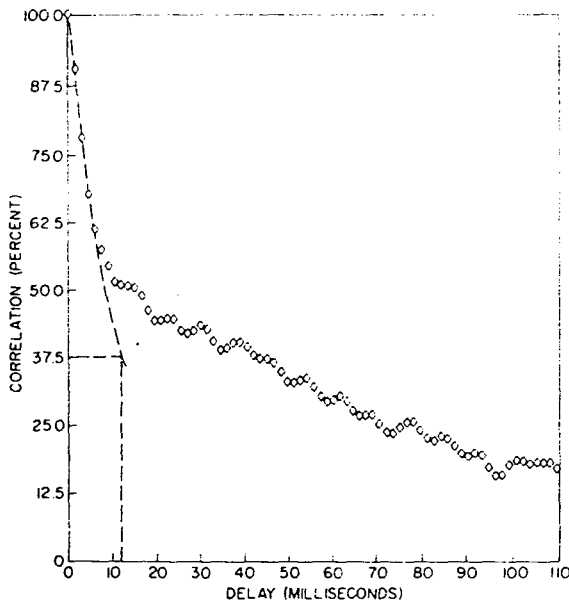


Fig. 7a—Normalized correlation of downwind rough-sea return of vertically polarized 20-nanosecond pulses at a 5° grazing angle

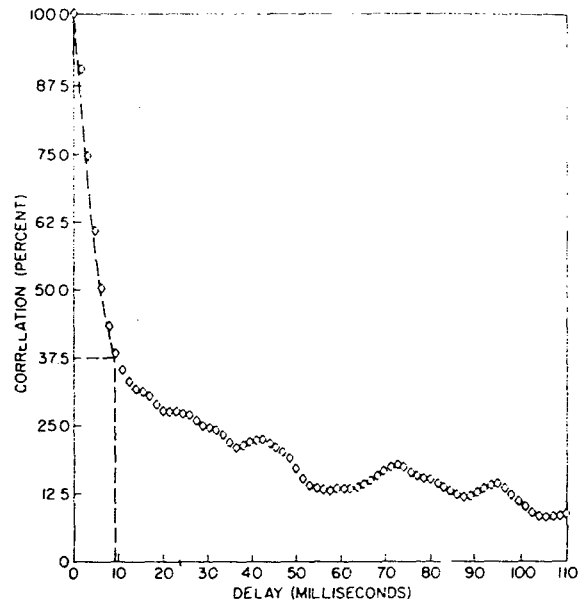


Fig. 7b—Normalized correlation of crosswind rough-sea return of vertically polarized 20-nanosecond pulses at a 5° grazing angle

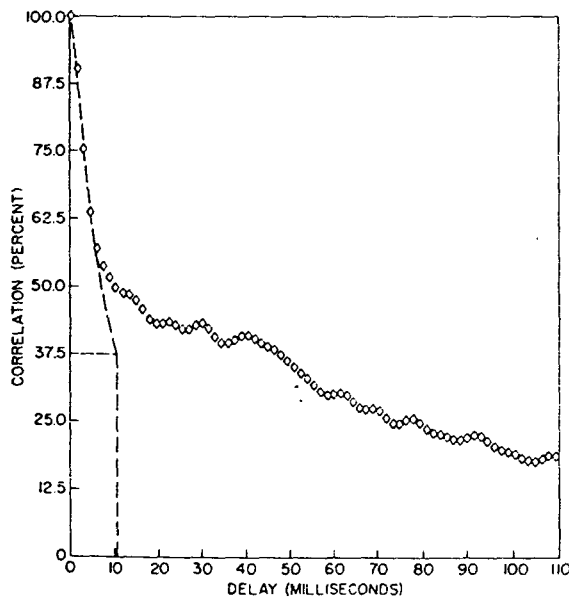


Fig. 7c—Normalized correlation of upwind rough-sea return of vertically polarized 20-nanosecond pulses at a 5° grazing angle

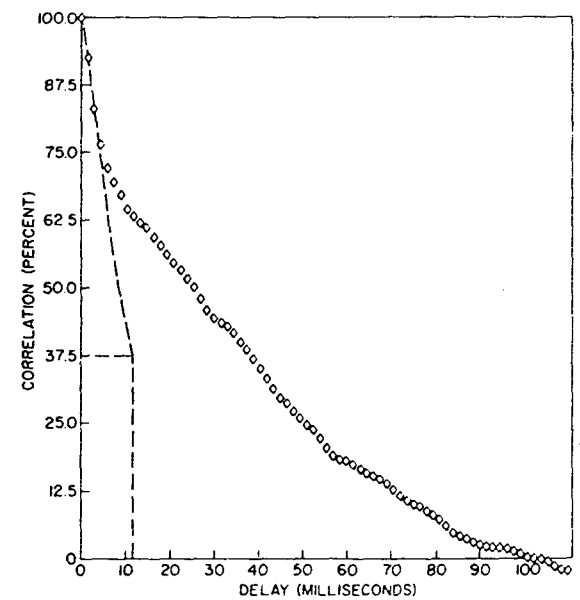


Fig. 7d—Normalized correlation of upwind rough-sea return of horizontally polarized 20-nanosecond pulses at a 5° grazing angle

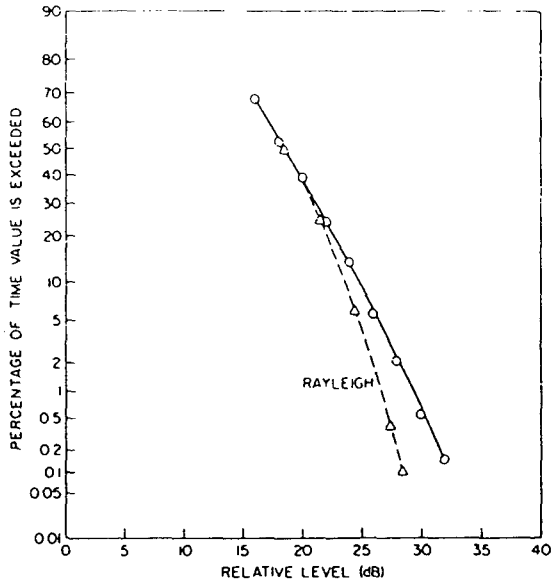


Fig. 8a—Amplitude distribution of downwind rough-sea return of vertically polarized 20-nanosecond pulses at a 5° grazing angle. The dynamic range to go in Table 2 is 14.0 dB.

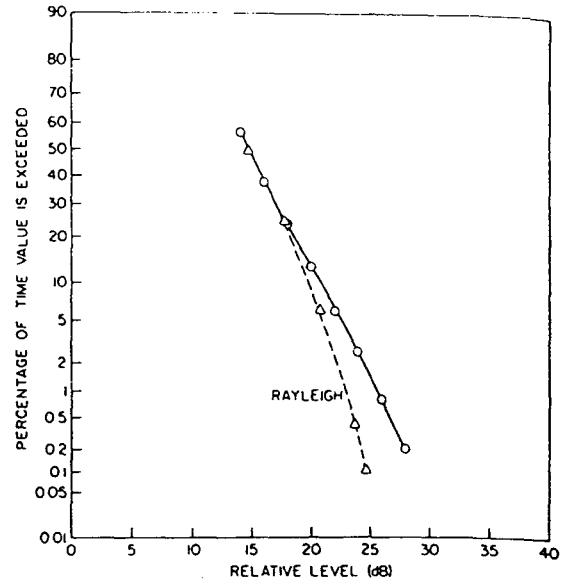


Fig. 8b—Amplitude distribution of crosswind rough-sea return of vertically polarized 20-nanosecond pulses at a 5° grazing angle. The dynamic range to go in Table 2 is 14.0 dB.

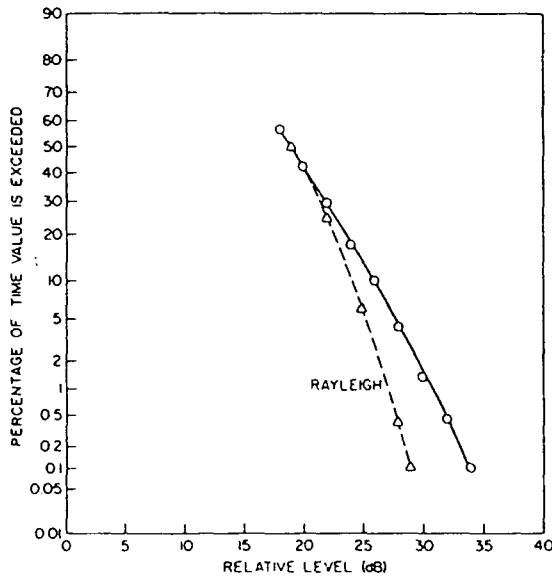


Fig. 8c—Amplitude distribution of upwind rough-sea return of vertically polarized 20-nanosecond pulses at a 5° grazing angle. The dynamic range to go in Table 2 is 15.0 dB.

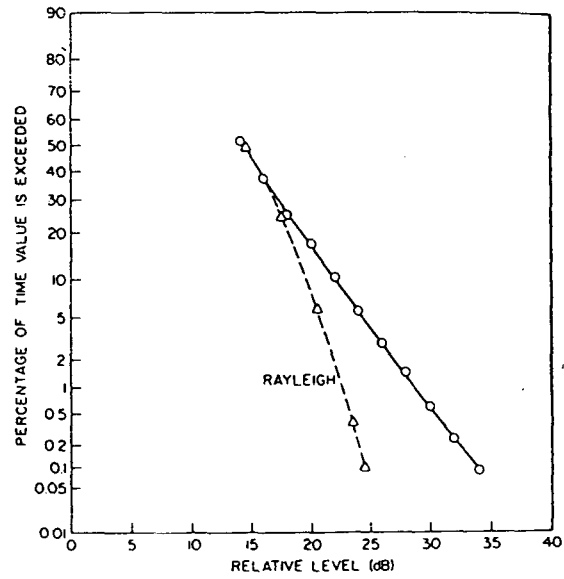


Fig. 8d—Amplitude distribution of upwind rough-sea return of horizontally polarized 20-nanosecond pulses at a 5° grazing angle. The dynamic range to go in Table 2 is 15.0 dB.

apparent lack of data at shorter pulses (<100 nsec) and narrow beamwidths mentioned in Ref. 9 which motivated our study of correlation at X band. Figures 7 indicate that for the upwind and downwind cases the long tail effect is prominent but for the crosswind case the correlation is more similar to the wider pulse UHF and S-band data discussed previously (9). Existing models do not account for these differences. The dashed lines on the figures indicate what the decorrelation distance would be if the function were smoothly decaying and the $1/e$ criteria were used.

Recent discussions with others who have observed the long tails with shore-based data indicate that at least three mechanisms must be taken into account in simulating the statistical properties of sea return (10). For the data described in this report, because of the tail structure of the correlation function, the number of independent samples per unit time is considerably less than what is obtained by employing the usual rule that decorrelation occurs in 10 to 20 milliseconds.

CONCLUSIONS AND FINAL REMARKS

Based on the data presented and analyzed here, the following conclusions are drawn with regard to the distribution functions:

- All curves are more skewed than the Rayleigh distribution.
- The curves for the horizontal polarization are more skewed than those for vertical polarization, with the differences being greater between the polarizations than for variations in any other parameter listed in Table 1.
- The departure from the Rayleigh is least for the crosswind cases.
- For vertical polarization the departure appears to increase for increasing sea roughness.
- Very little difference is noted between the two pulse widths except for the anticipated 7-dB higher mean level for the wider pulse.
- None of the airborne results is a worst case with regard to the departure from the Rayleigh, which is demonstrated by the very-low-angle (0.3 degree) example.

The following conclusions are drawn with regard to the autocorrelation functions:

- Decorrelation time in the usual sense has little meaning except possibly for crosswind conditions.
- As was the case with the distributions, the greatest differences occur between the polarizations rather than for variations in any other parameter.

Although the correlation functions strongly indicate a multimechanism scattering phenomenon, the non-Rayleigh nature of the distribution of swimming pool clutter from fine-structured fan-generated waves indicates that the particular composite surface mentioned earlier is an insufficient explanation. Swimming-pool or wave-tank measurements with controllable wind speeds and grazing angles should be encouraged, since they would provide needed additional insight before a satisfactory scattering model emerges.

ACKNOWLEDGMENTS

We thank G. F. Myers and the other members of the Radar Geophysics Branch who provided the pool clutter data. We also thank N. L. Davis for his helpful suggestions while directing the research program.

REFERENCES

1. J.R. Wait, editor, "Electromagnetic Probing in Geophysics," The Golem Press, Boulder, Colorado, 1971.
2. P. Beckmann, and A. Spizzichino, "The Scattering of Electromagnetic Waves from Rough Surfaces," New York, Pergamon Press, 1963.
3. K.R. Schmidt, "Statistical Time-Varying and Distribution Properties of High-Resolution Radar Sea Echo," NRL Report 7150, Nov. 1970.
4. J.C. Daley, W.T. Davis, and N.R. Mills, "Radar Sea Return in High Sea States," NRL Report 7142, Sept. 1970.
5. M.L. Shumaker, "A Frequency-Agile High-Resolution Radar," NRL Memorandum Report 2026, Aug. 1969.
6. A.M. Findlay, "Decorrelation of Sea Clutter by Radar Frequency Agility, Part I," NRL Memorandum Report 2136, June 1970.
7. G.F. Myers, and I.W. Fuller, Jr., "Nanosecond Radar Observations of Sea Clutter Cross-Section vs Grazing Angle," NRL Report 6933, Oct. 1969.
8. M.S. Longuet-Higgins, "The Effect of Non-Linearities on Statistical Distributions in the Theory of Sea Waves," J. Fluid Mechanics 17, 459-480 (Nov. 1963).
9. F.E. Nathanson, "Radar Design Principles; Signal Processing and the Environment," New York, McGraw-Hill, 1969, pp. 249-253.
10. W.K. Rivers, Engineering Experiment Station, Georgia Institute of Technology, private communication.

Security Classification		
DOCUMENT CONTROL DATA - R & D		
<small>(Security classification of title, body of abstract and indexing annotation must be entered when the overall report is classified)</small>		
1. ORIGINATING ACTIVITY (Corporate author) Naval Research Laboratory Washington, D.C. 20390	2a. REPORT SECURITY CLASSIFICATION Unclassified	
	2b. GROUP	
3. REPORT TITLE STATISTICAL FUNCTIONS OF SHORT-PULSE RADAR SEA RETURN		
4. DESCRIPTIVE NOTES (Type of report and inclusive dates) Interim report on a continuing NRL problem		
5. AUTHOR(S) (First name, middle initial, last name) K. R. Schmidt, P. M. Thiebaud, and S. J. Weller		
6. REPORT DATE July 26, 1972	7a. TOTAL NO. OF PAGES 20	7b. NO. OF REFS 10
8a. CONTRACT OR GRANT NO NRL Problem R02-34A b. PROJECT NO RF 12-151-403-4008 c. d.	9a. ORIGINATOR'S REPORT NUMBER(S) NRL Report 7420 9b. OTHER REPORT NO(S) (Any other numbers that may be assigned this report)	
10. DISTRIBUTION STATEMENT Approved for public release; distribution unlimited.		
11. SUPPLEMENTARY NOTES	12. SPONSORING MILITARY ACTIVITY Department of the Navy Office of Naval Research Arlington, Virginia 22217	
13. ABSTRACT <p>This report presents and discusses experimental results of short-pulse (20 and 100 nsec) X-band radar backscatter measurements from rough water surfaces. The emphasis is on airborne open-ocean conditions, but some results from very-low-angle shore-based data and 1-nanosecond radar measurements in the NRL swimming pool are also shown. The experimental data are in the form of cumulative probability distribution functions and autocorrelation functions. Among the various conclusions drawn are that the non-Rayleigh character of the data cannot be adequately explained by a composite surface which consists of a slightly rough, ideal Gaussian random surface superimposed upon a wave structure whose crest-to-trough amplitude is very large compared to a radar wavelength. The pool clutter results indicate that such a large wave structure is not necessary to obtain data which are considerably more skewed than Rayleigh. Additional wave-tank measurements should be made to gain insight as to the effects of the variation of many of the parameters which in the present study remain fixed.</p>		

Security Classification						
14. KEY WORDS	LINK A		LINK B		LINK C	
	ROLE	WT	ROLE	WT	ROLE	WT
Surface roughness						
Sea clutter						
Backscattering						
Short pulse radar						
High resolution radar						
Radar echoes						
Statistical distributions						
Skewness						
Autocorrelation						
Ocean waves						
Radar surveillance						
Airborne radar						
Radar detection						